Pharm Res (2014) 31:3371–3378
DOI 10.1007/s11095-014-1426-z

RESEARCH PAPER

Fluorescent Dye Labeled Iron Oxide/Silica Core/Shell Nanoparticle as a Multimodal Imaging Probe

Eue Soon Jang • Seung Yong Lee • Eui-Joon Cha • In-Cheol Sun • Ick Chan Kwon • Dukjoon Kim • Young Il Kim • Kwangmeyung Kim • Cheol-Hee Ahn

Received: 11 March 2014 / Accepted: 12 May 2014 / Published online: 31 May 2014

ABSTRACT

Purpose To develop an MRI/optical multimodal imaging probe based on dye-conjugated iron oxide/silica core/shell nanoparticle, and investigate the distance-dependent fluorescence quenching through careful control of the distance between the iron oxide core and fluorescent dyes.

Methods Different size of core/shell nanoparticles were prepared by varying the silica shell width. PEGylation on the surface of silica shell was followed to improve the stability of particles in the physiological condition. *In vitro* cytotoxicity was evaluated by the MTT assay on a HeLa cell line and *in vivo* imaging of subcutaneous SCC7 xenografted mice was performed using MRI/optical imaging modalities.

Results Diameter and ζ-potential of the nanoparticles were measured, and TEM images demonstrated the mono-disperse nature of the particles. Quenching efficiency of the dyes on the surface was nearly 100% in the smallest nanoparticle, while almost no quenching effect was observed for the largest nanoparticle. *In vitro* cytotoxicity showed nearly 90% cell viability at 0.15 Fe mg/mL, a comparable concentration for clinical use. The tumor area was significantly darkened after the nanoparticle injection due to the high transverse relaxivity value of the nanoparticles. Fluorescence signal was affected by the particle size due to the distance-dependent quenching/dequenching behaviour.

KEY WORDS Core-shell nanoparticle · Fluorescence quenching · Iron oxide · Multimodal imaging probe · Optical imaging

ABBREVIATIONS

APTES	3-aminopropyl triethoxysilane
Cy	Cyanine
CY-CS	Cy-conjugated CS

These authors Eue Soon Jang and Seung Yong Lee are contributed equally to this paper

Electronic supplementary material The online version of this article (doi:10.1007/s11095-014-1426-z) contains supplementary material, which is available to authorized users.

E. S. Jang
Advanced Materials Educational Institute, Kumoh National Institute of Technology, Sanho-ro 77, Yangho, Gumi 730-701, South Korea

S. Y. Lee • E.-J. Cha • C.-H. Ahn
Research Institute of Advanced Materials (RIAM), Department of Materials Science and Engineering, Seoul National University San 56-1, SillimGwanak Seoul 151-744, South Korea

I.-C. Sun • K. Kim
Biomedical Research Center, Korea Institute of Science and Technology (KIST), 39-1, HawolgokSeongbuk Seoul 136-791, South Korea

I. C. Kwon
Department of Chemical Engineering, Theranostic Macromolecule Research Center, Sungkyunkwan University, Suwon Kyunggi 440-746, South Korea

D. Kim • Y. I. Kim
Department of Radiology, Seoul National University Hospital 28, YeongeonJongno Seoul 110-744, South Korea

C.-H. Ahn (✉)
Materials Science and Engineering, Seoul National UniversitySeoul 151-744, South Korea
e-mail: chahn@snu.ac.kr

K. Kim (✉)
Biomedical Research Center, Korea Institute of Science and Technology, Seoul 136-791, South Korea
e-mail: kim@kist.re.kr

Y. I. Kim (✉)
Radiology, Seoul National University Hospital, Seoul 110-744 South Korea
e-mail: kyimd@snu.ac.kr

CS	Core-shell
DMEM	Dulbecco's modified eagle medium
EDC	Ethyl (dimethylaminopropyl) carbodiimide
FBS	Fetal bovine serum
FRET	Fluorescence resonance energy transfer
HF	Hydrofluoric acid
ICP-MS	Inductively coupled plasma mass spectrometry
mPEG-COOH	Methoxy poly (ethylene glycol) mono acid
MRI	Magnetic resonance imaging
MTT	Methylthiazol tetrazolium
NIRF	Near-infrared fluorescence
NHS	*N*-hydroxysuccinimide
PL	Photoluminescence
TEM	Transmission electron microscopy

INTRODUCTION

Magnetic resonance imaging (MRI) and optical imaging are two highly complementary techniques, one providing anatomical details (1–4) and the other delivering functional and biological information on molecular levels (5–7). The combination of two modalities to develop a multimodal molecular imaging probe complements the weaknesses present in each system and provides clinicians with a definitive tool for identification and characterization of specific targets in living subjects' anatomical context (8).

In the course of developing multimodal contrast agents based on iron oxide nanoparticles, (9–15) researchers have reported that iron oxide has the ability to quench fluorescent materials (16–21). Weissleder *et al.* reported fluorescence quenching by iron oxide and fabricated a magnetic nanoparticle-based MRI contrast agent that was enzyme-triggered to produce near-infrared fluorescence (NIRF) imaging (16). They claimed that the fluorescence quenching of magnetic nanoparticles might be due to nonradiative energy transfer between the fluorescent dyes and iron oxide, or to the collisions between dyes and the nanoparticles. Zhang *et al.* demonstrated fabrication method for bifunctional magnetic nanoparticle using silica shell to induce fluorescence quenching by iron oxide core within a confined space (20). There are several hypotheses to explain fluorescence quenching by iron oxides, among which are 1) electron coupling effect between iron oxide and the fluorescent dye and 2) broad absorption by iron oxide (20). The first mechanism is through which gold nanoparticles quench fluorescence (17, 22); some researchers have assumed that iron oxide quenches fluorescence through the same mechanism (21). However, Nie *et al.* has demonstrated that fluorescence quenching could be still observed in dilute solutions of iron oxide and quantum dot, in which iron oxide and the dye are not in direct contact (19), thereby suggesting that iron oxide quenches fluorescence through a different mechanism rather than energy transfer through electron coupling. In spite of researches on iron oxide nanoparticles, the mechanism behind fluorescence quenching by iron oxide has not been clearly elucidated.

In this study, we demonstrate the distance-dependent fluorescence quenching by iron oxide core-shell (CS) nanoparticle through careful control of the distance between the iron oxide core and the fluorescent dyes by varying the silica shell width. The fluorescence quenching mechanism of iron oxide was not suggested, but systematic approach to give a qualitative guideline for quenching/dequenching of the fluorophores was experimentally investigated and the results opened the possibility to precisely design a stimuli-activatable multimodal molecular imaging probes based on MR and optical imaging.

MATERIALS AND METHODS

Iron Oxide/Silica Core/Shell (CS) Nanoparticles

Silica coating coated onto the surface of the hydrophobic iron oxide nanoparticles with oleic acid ligand was accomplished by modified reverse microemulsion procedure (23). Different volume (10, 20, 60, and 300 μL) of iron oxide nanoparticles (13 nm, 10 mg Fe/mL) was dispersed into 60 mL cyclohexane. Triton-X 100 (1.12 mL), 1-octanol (400 μL), tetraethyl orthosilicate (TEOS, 200 μL) and NH_4OH (152.8 μL) were added into each solution and the reaction was continued for 3 days at 600 rpm. The reaction mixture was then dispersed into 60 mL anhydrous EtOH after washing with EtOH through centrifugation at 20,000 rpm for 30 min. Silica thickness, confirmed by transmission electron microscopy (TEM), was controlled from 42 to 4.6 nm by increasing the initial concentration of the iron oxide nanoparticles from 10 to 300 μL. The codes were assigned according to the CS particle diameters; CS20 (20.2 nm), CS33 (32.6 nm), CS60 (59.2 nm), and CS113 (113.8 nm). The final concentrations of nanoparticles in anhydrous EtOH, determined by inductively coupled plasma mass spectrometry (ICP-MS) analysis, were 56.3, 51.0, 44.8, and 45.8 μg Fe per mL for CS20, CS33, CS60, and CS113, respectively. Measurements of ζ-potential and particle size were carried out using ELS-Z system (Otsuka electronics Co. Ltd., Osaka, Japan) equipped with He-Ne laser at a wavelength of 630 nm.

Cy-Conjugated CS (CY-CS) and PEGylated Nanoparticles (PEGylated CY-CS)

1.0 mL 3-aminopropyl triethoxysilane (APTES) was added to 10.0 mL EtOH solution of the CS nanoparticles to introduce amine groups on the surface. Vigorous stirring the mixture was continued for 12 h at room temperature and unreacted

APTES was removed by 5 times centrifugation against anhydrous EtOH. The aminated CS nanoparticles were redispersed into deionized water.

Cy 5.5 mono acid (0.1 mg) and 1.0 mg EDC/NHS were dissolved in 1.0 mL deionized water and added to 5.0 mL of aminated CS nanoparticle solution. The reaction was carried out in darkness for 12 h with vigorous stirring. The final product was dispersed into 5.0 mL deionized water after washing with distilled water through 5 times centrifugation at 13,000 rpm to remove unreacted reactants. Cy-conjugated CS nanoparticles were coded as CY-CS20, CY-CS33, CY-CS60, and CY-CS113.

Methoxy poly (ethylene glycol) mono acid (mPEG-COOH) (1.0 mg) activated by NHS was added into 5.0 mL of aminated CY-CS nanoparticles in deionized water and the solution was stirred vigorously at room temperature. After 3 h reaction, PEGylated CY-CS nanoparticles were centrifuged 3 times with deionized water at 14,500 rpm for 30 min and redispersed in 5.0 mL of deionized water for the further experiments.

Determination of Quenching Efficiency

For the evaluation of quenching efficiency of conjugated dyes on the surface of the nanoparticles, photoluminescence (PL) intensities of intact CY-CS nanoparticles were compared to those of hydrofluoric acid (HF) treated nanoparticles. 5.0 mL CY-CS nanoparticles were mixed with 5.0 mL HF in a 50 mL poly (tetrafluoroethylene) (PTFE) beaker and the reaction mixtures were stirred for 3 h to completely decompose silica shell and to free the Cy dyes from the surface of nanoparticles. Residual HF and by-products were removed by evaporation with 60.0 mL distilled water 3 times at 160°C. Cy dyes freed from the surface of nanoparticles were dissolved in 5.0 mL deionized water and their PL intensities as well as those of CY-CS nanoparticles were measured using a Shimadzu spectrophotometer and Kodak imaging station system (Kodak, New Haven, CT) with 4000MM charge coupled device (CCD) camera and Cy emission filter.

Measurement of Relaxivity

Magnetic resonance imaging studies were carried out using a MRI scanner at 3 T field strength and transverse relaxation time (T2) of each nanoparticle was obtained at room temperature and 60 Hz. The T2 relaxivity of each sample was calculated by fitting the 1/T2 (r2) values *versus* iron contents of the CS nanoparticles according to the equation of $T2 = 1/(A\,[Fe])$, where T2 is the transverse relaxation time at a given iron concentration, [Fe] and A is the relaxivity of the CS nanoparticles.

In Vitro Cytotoxicity

In Vitro. cytotoxicity of nanoparticles was evaluated using methylthiazol tetrazolium (MTT) assay (24). HeLa cells were grown in each well of 96-well plates containing 0.2 mL Dulbecco's modified eagle medium (DMEM) with 10% fetal bovine serum (FBS). Cells were washed with pre-warmed phosphate buffered saline (PBS) and incubated with pre-warmed DMEM for 30 min before the addition of CY-CS and PEGylated CY-CS nanoparticles. After cells were incubated for 4 h at 37°C in nanoparticle-dispersed DMEM, the medium was replaced by fresh DMEM without serum. 0.1 mL MTT solution (1 mg/mL) was added to each well and cells were incubated for an additional 4 h. Medium was removed and 0.2 mL dimethyl sulfoxide (DMSO) was added to dissolve the formazan crystal. Fluorescence of solution was measured at 570 nm using a micro-plate reader.

In Vivo Magnetic Resonance Imaging (MRI) and Near Infrared Fluorescence Imaging (NIRF)

For *in vivo* visualization of the nanoparticles, squamous cell carcinoma (SCC7) cells cultured in Roswell park memorial institute (RPMI) 1640 medium with 10% FBS were inoculated into the back of BALB/C nude mouse by subcutaneous injection. When tumor had grown up, 0.3 mL PEGylated CY-CS20 and PEGylated CY-CS113 (0.15 Fe mg/mL) was injected intratumorally and images were obtained by two different imaging modalities, MR and NIRF tomographic image. MR images were obtained using a MRI scanner at 3.0-T field strength (Tim Trio; Siemens, Erlangen, Germany). Mice were placed on the tray of the MRI scanner and imaged before/after the injection. T2-weighted MR images were obtained by a multi-spin echo multi-slice imaging sequence with following parameters: TR = 51 ms, TE = 20 ms and slice thickness of 0.6 mm. NIRF tomographic images were obtained with an eXplore Optix system (Advanced Research Technologies Inc., Montreal, Canada). The fluorescence in SCC7 tumor-bearing mice were imaged using the eXplore Optix system with laser power and integration time of 10 μW and 0.3 s. A 670 nm laser was applied to excite Cy dyes and 700 nm emission filters was applied to collect fluorescence emission of Cy. After NIRF imaging, mice were sacrificed and the NIRF images of excised tumor was obtained using a Kodak Image Station 4000MM Digital Imaging System.

RESULTS AND DISCUSSION

To study the effect of distance between the surface of nanoparticles and the fluorescent dyes on the quenching efficiency, four samples were made with varying thickness of silica shell

on iron oxide core. Scheme of the preparation is illustrated in Fig. 1. Diameters of CS nanoparticles measured by dynamic light scattering were 20.2 (CS20), 32.6 (CS33), 59.2 (CS60), and 113.8 nm (CS113). The ζ-potential values of the samples were −3.3, −5.3, −16.2, and −29.3 mV, respectively. The negative ζ-potential values indicate that silica shell was successfully coated on the surface of the core and the increasing values were well matched to the corresponding thickness of the shell. The samples were mono-dispersed, as demonstrated by TEM images, except for the case of CS113, which showed relatively broader distribution due to the experimental difficulty in introducing thicker silica layer. TEM images clearly showed the spherical core-shell structures with single iron oxide core and the silica shell with precisely controlled thickness (Fig. 2).

Fluorescent Cy dyes were conjugated on the silica surface to produce multimodal nanoparticular imaging probes, CY-CS. PL spectra of the CY-CS were measured to study the effect of distance between dyes and iron oxide core on quenching efficiency (Fig. 3a). CY-CS were treated with HF to decompose the silica shell and to free dyes from the surface of the nanoparticles, which induced the full fluorescence recovery of Cy dyes conjugated on the nanoparticles, as illustrated in Fig. 1. The PL intensity of Cy dyes was not affected during the shell-dissolving process by the presence of HF (Fig. 3b). Quenching efficiency was defined as (PL intensity of HF treated CY-CS nanoparticle − PL intensity of CY-CS nanoparticle)/(PL intensity of HF treated CY-CS nanoparticle) * 100. The PL intensity of each sample was measured 3 times and averaged values were used for the calculation of quenching efficiency. In order to make sure that the quenching behavior did not stem from fluorescence resonance energy transfer (FRET) between Cy dyes, the average number of Cy molecules on each particle was calculated based on the surface area of nanoparticles, the number of nanoparticles and Cy dyes in nanoparticle solution. Table I summarizes the results and the possible self-quenching of Cy dyes via FRET mechanism was ruled out from the calculation of average distance between the dyes in each sample, since the distance was larger than maximum Förster radius in Cy molecules, which is around 10 nm (25, 26). Quenching efficiency was nearly 100% in CY-CS20 while almost no quenching effect was observed for the case of CY-CS113. NIRF image of CY-CS in Fig. 3(c) supports the results. The quenching efficiency was gradually decreased with corresponding increase in the thickness of silica shell and this result shows that the fluorescence quenching property of iron oxide was influenced by distance between Cy dyes and iron oxide and the quenching behavior could be controlled by changing the thickness of silica shell.

CS-CY were PEGylated for enhanced stability in aqueous condition. Diameters of PEGylated CS-CY nanoparticles by dynamic light scattering measurements increased

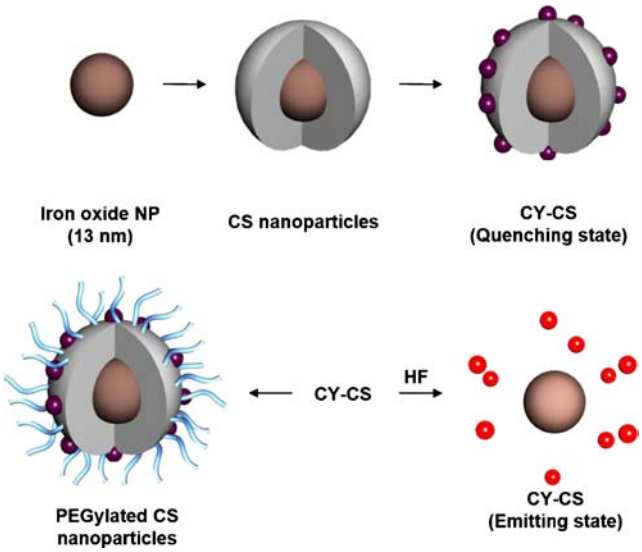

Fig. 1 Schematic diagram of dye-conjugated PEGylated CY-CS preparation and HF treated CY-CS.

to be 26.5, 41.2, 68.1 and 134.4 nm from CY-CS20, 33, 60 and 113, respectively, due to the hydrophilic nature of PEG. Transverse relaxation time was measured using MRI scanner at 3 T magnetic field strength to evaluate the use of PEGylated CY-CS nanoparticles as MRI a contrast agent. Transverse relaxivity (r2) value of all the PEGylated CY-CS nanoparticles was higher than that of Feridex, clinically used iron oxide based MRI contrast agent and gradually decreased with increasing the silica shell thickness (Fig. SI.1) (27). High relaxivity values and distance-dependent quenching/dequenching behaviour make the CY-CS nanoparticles be an activatable multimodal nanoparticular imaging probes when stimuli-sensitive degradable groups are introduced to connect the dyes and iron oxide nanoparticles.

In Vitro. cytotoxicity of CY-CS and PEGylated CY-CS nanoparticles was evaluated by the MTT assay on a HeLa cell line (Fig. 4) and PEGylated CY-CS-treated cells showed higher viability than CY-CS-treated cells. Surface modification of iron oxide nanoparticles, using silica and PEG, enhanced the aqueous stability and reduced the cytotoxicity of the nanoparticles. In a number of *in vivo* reports for MR studies using nude mice, 0.03 ~ 0.05 mL iron oxide nanoparticles with the iron concentration of 0.1 ~ 0.3 Fe mg/mL was injected intravenously, which corresponds to 0.25 ~ 0.75 Fe mg/kg assuming the weight of a mouse is around 13 g. Injection dose of Feridex, dextran-coated iron oxide nanoparticles clinically in use as a MR contrast agent, is 0.56 Fe mg/kg in 100 mL of 5% dextrose solution (28). PEGylated CY-CS nanoparticles showed nearly 90% cell viability at the concentration of 0.15 Fe mg/mL, which is a comparable concentration for *in vivo* study and clinical use. Considering these results, the

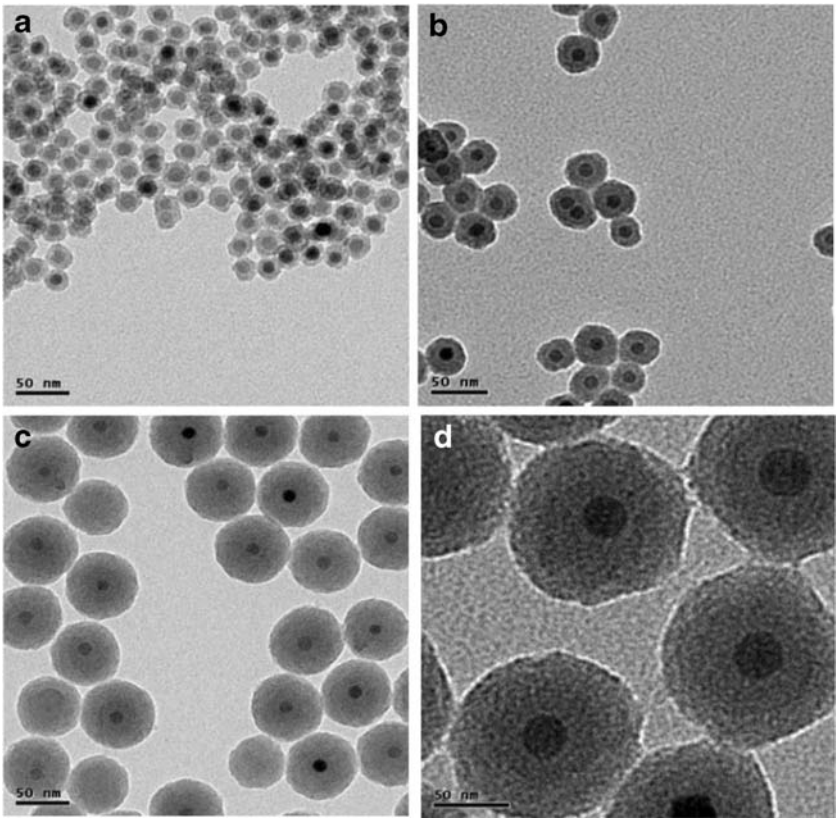

Fig. 2 TEM images of CS nanoparticles. (**a**) CS20, (**b**) CS33, (**c**) CS60, and (**d**) CS113.

cytotoxicity of PEGylated CY-CS nanoparticles were low enough to make the nanoparticles an excellent candidate for *in vivo* applications.

In Vivo. imaging of subcutaneous SCC7 xenografted mice was performed using two different imaging modalities, MR imaging and NIRF tomographic imaging. PEGylated CY-CS20 and PEGylated CY-CS113 were intratumorally injected and imaged by Tim Trio MRI scanning system. As shown in Fig. 5(a), the tumor area was significantly darkened after the nanoparticle injection due to the high transverse relaxivity value of the nanoparticle. The relative signal enhancement was 41.5±6.69% for the case of PEGylated CY-CS20 and 31.2±3.77% for PEGylated CY-CS113, respectively. The relative signal enhancement of the ROI in the T2-weighted image was obtained by the comparison of signal intensity between the tumor site and the healthy muscles. Intratumorally injected nanoparticles remain mostly in the extracellular matrix, where the diffusion of nanoparticles is generally limited. As shown in Fig. 5(a), dark and bright region co-existed in the tumor site since the injected nanoparticles did not fully diffuse into the whole tumor region. After MRI scanning, NIRF tomographic image was evaluated by eXplore Optix system using NIRF probe detection setting with excitation and emission at 670 nm and 700 nm, respectively. As shown in Fig. 5(b), weak fluorescence signal was detected in PEGylated CY-CS20 injected tumor-bearing mouse, while the mouse with PEGylated CY-CS113 produced strong fluorescence signals in the injected site due to the previously discussed distance-dependent quenching/dequenching behaviour of PEGylated CY-CS nanoparticles. Fig. 5(c) depicts NIRF images of excised tumors. PEGylated CY-CS113 injected tumor produced strong fluorescence signal and PEGylated CY-CS20 administered tumor showed weak fluorescence signal, which was in a good agreement with *in vivo* imaging results. NIRF signal in tumor was not uniformly distributed probably due to the limited diffusion of the nanoparticles in the extracellular space as described in the MR imaging. Fig. 5 supported that multimodal nanoparticular imaging probes were successfully prepared and distance-dependent quenching/dequenching properties opened a strong possibility of PEGylated CY-CS nanoparticles as an on/off imaging probe activated by an external stimuli which free the Cy dyes from the surface of the nanoparticles under a specific condition.

CONCLUSION

Core/shell nanoparticles consisting of iron oxide core and silica shell with different thickness were successfully prepared.

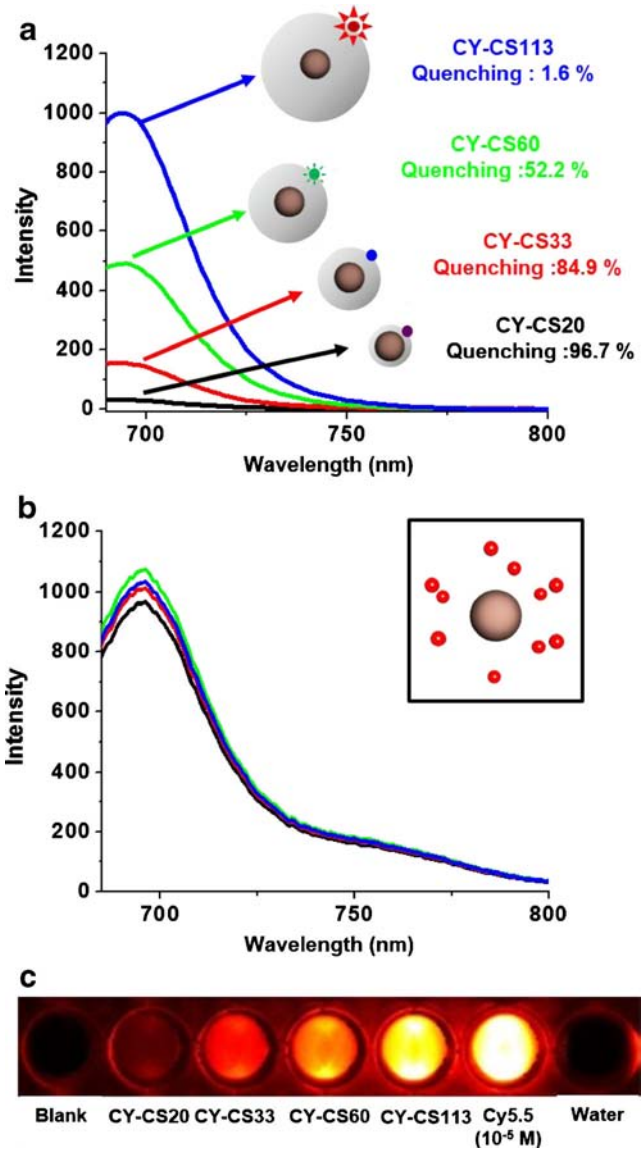

Fig. 3 PL spectra of CY-CS (**a**) before HF treatment. (**b**) after HF treatment and (**c**) NIRF image of CY-CS.

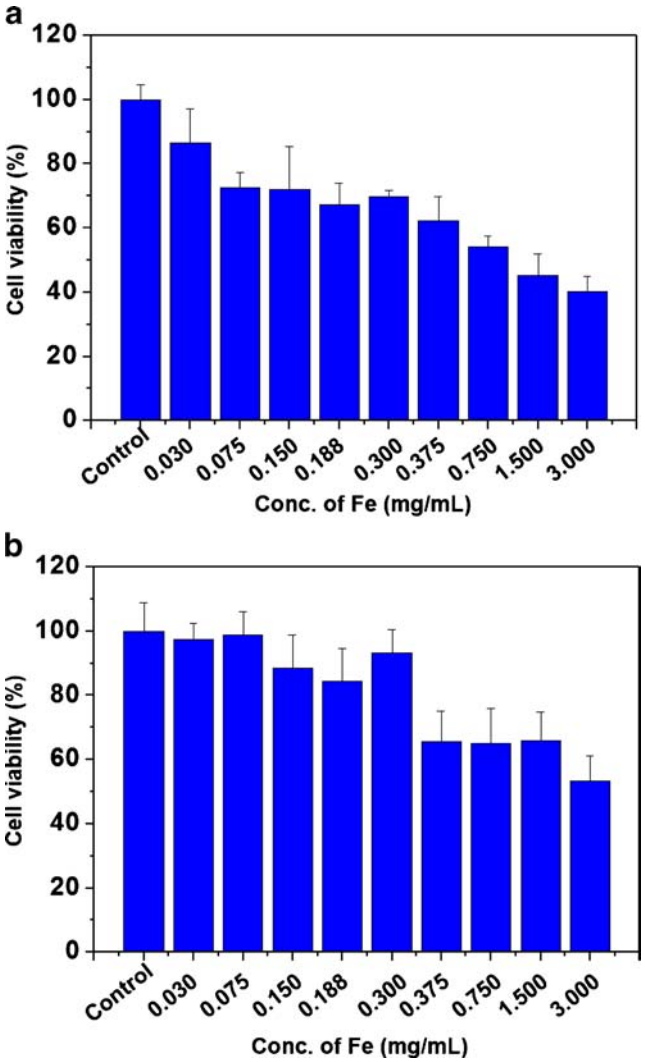

Fig. 4 Cell viability of (**a**) CY-CS20 and (**b**) PEGylated CY-CS20.

The nanoparticles were conjugated with fluorescent Cy dyes and PEGylated to enhance the stability in the aqueous condition. Quenching effect of the conjugated dyes was investigated as a function of the distance between dyes and the surface of nanoparticles. Dyes were almost perfectly quenched when located within 10 nm from the surface and the quenching effect decreased as the distance increased, which resulted in nearly no quenching effect with PEGylated CY-CS113 nanoparticles. Based on the calculation of the number of dyes on the nanoparticles, the quenching effect

Table I PL intensity of CY-CS nanoparticles with/without HF treatment, number of Cy dyes on a particle and quenching efficiency

Sample	Fluorescence intensity of CY-CS[a]		Cy5.5/particle	Quenching efficiency (%)
	Intact	HF treated		
CY-CS20	31.1	942.1	6.22	96.7
CY-CS33	149.5	988.2	7.59	84.9
CY-CS60	500.4	1,046.6	17.86	52.2
CY-CS113	991.2	1,007.4	42.46	1.6

[a] PL measurement at 692 nm

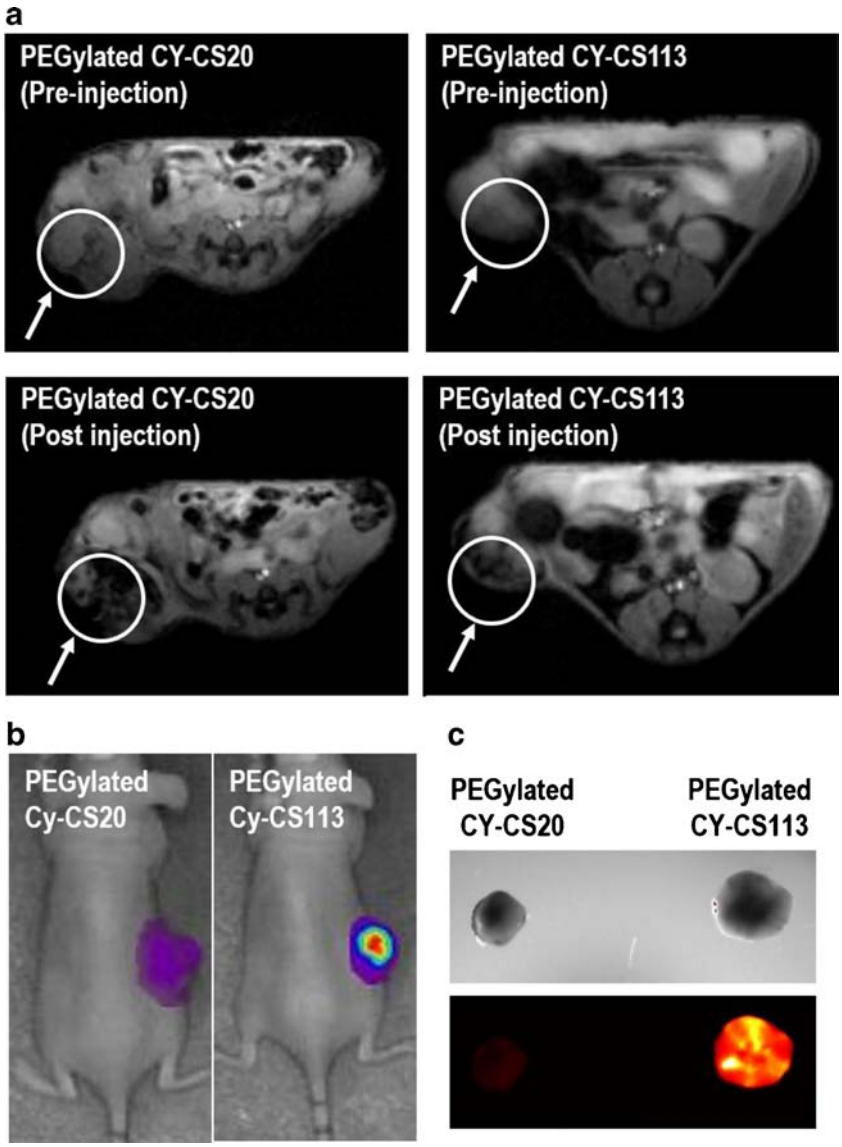

Fig. 5 *In vivo* (**a**) MR, (**b**) NIRF image and (**c**) NIRF image of excised tumor with PEGylated CY-CS20 and PEGylated CY-CS113.

was not from FRET mechanism between dyes, but stem from the distance effect from the nanoparticles. These results helps the design of activatable optical nanoparticular imaging probes even though the detailed mechanism of quenching is not studied in this research.

PEGylated CY-CS nanoparticles were not cytotoxic at the concentration of iron which is clinically in use and other *in vivo* reports. The nanoparticles showed higher relaxivity values than that of Feridex, clinically used iron oxide based MR contrast agent, and produce a good T2-weighted MR images *in vivo*. PEGylated CY-CS113 nanoparticles were successfully imaged optically *in vivo* and the results proved that the nanoparticles in this study are useful in developing a multimodal imaging contrast agent. The probes can be developed as an activatable optical imaging contrast agent with proper conjugation of the dyes utilizing a connecting part that can be triggered to be composed and to release the fluorescent dyes in response to a corresponding environmental stimuli. In conclusion, PEGylated CY-CS nanoparticles highlight the great potential as an effective multimodal imaging contrast agent and the quenching effect was systemically investigated with the distance between the dye and the nanoparticles as a variable.

ACKNOWLEDGMENTS AND DISCLOSURES

This study was supported by a grant from Basic Science Research Program (grant no. 2010–0027955) of MEST and National Research Foundation of Korea (grant no. 2010–0023581). C.-H. Ahn appreciate LG Yonam Foundation for the support.

REFERENCES

1. Y-w J, Lee JH. Cheon J. Chemical Design of Nanoparticle Probes for High-Performance Magnetic Resonance Imaging. Angew Chem Int Ed. 2008;47(28):5122–35.
2. Rudin M, Weissleder R. Molecular Imaging in Drug Discovery and Development. Nat Rev Drug Discov. 2003;2(2):123–31.
3. Smith RE, Tournier JD, Calamante F, Connelly A. Anatomically-Constrained Tractography: Improved Diffusion MRI Streamlines Tractography Through Effective use of Anatomical Information. NeuroImage. 2012;62(3):1924–38.
4. Abdalla MO, Karna P, Sajja HK, Mao H, Yates C, Turner T, *et al.* Enhanced Noscapine Delivery Using uPAR-Targeted Optical-MR Imaging Trackable Nanoparticles for Prostate Cancer Therapy. J Control Release. 2011;149(3):314–22.
5. Kutscher HL, Chao P, Deshmukh M, Singh Y, Hu P, Joseph LB, *et al.* Threshold Size for Optimal Passive Pulmonary Targeting and Retention of Rigid Microparticles in Rats. J Control Release. 2010;143(1):31–7.
6. Rosi NL, Giljohann DA, Thaxton CS, Lytton-Jean AKR, Han MS, Mirkin CA. Oligonucleotide-Modified Gold Nanoparticles for Intracellular Gene Regulation. Science. 2006;312(5776):1027–30.
7. Huang X, El-Sayed IH, Qian W, El-Sayed MA. Cancer Cell Imaging and Photothermal Therapy in the Near-Infrared Region by Using Gold Nanorods. J Am Chem Soc. 2006;128(6):2115–20.
8. Sun IC, Eun DK, Koo H, Ko CY, Kim HS, Yi DK, *et al.* Tumor-Targeting Gold Particles for Dual Computed Tomography/Optical Cancer Imaging. Angew Chem Int Ed. 2011;50(40):9348–51.
9. Shin J, Anisur RM, Ko MK, Im GH, Lee JH, Lee IS. Hollow Manganese Oxide Nanoparticles as Multifunctional Agents for Magnetic Resonance Imaging and Drug Delivery. Angew Chem Int Ed. 2009;48(2):321–4.
10. Kim J, Kim HS, Lee N, Kim T, Kim H, Yu T, *et al.* Multifunctional Uniform Nanoparticles Composed of a Magnetite Nanocrystal Core and a Mesoporous Silica Shell for Magnetic Resonance and Fluorescence Imaging and for Drug Delivery. Angew Chem Int Ed. 2008;47(44):8438–41.
11. Yu MK, Jeong YY, Park J, Park S, Kim JW, Min JJ, *et al.* Drug-Loaded Superparamagnetic Iron Oxide Nanoparticles for Combined Cancer Imaging and Therapy *In Vivo*. Angew Chem Int Ed. 2008;47(29):5362–5.
12. Choi J, Lee S, Kang HJ, Lee J, Kim J, Yoo HO, *et al.* Synthesis of Water-Soluble Chitosan-g-PEO and its Application for Preparation of Superparamagnetic Iron Oxide Nanoparticles in Aqueous Media. Macromol Res. 2010;18(5):504–11.
13. Selim KMK, Lee JH, Kim SJ, Xing Z, Kang IK, Chang Y, *et al.* Surface Modification of Magnetites Using Maltotrionic Acid and Folic Acid for Molecular Imaging. Macromol Res. 2006;14(6):646–53.
14. Kim J, Park S, Lee JE, Jin SM, Lee JH, Lee IS, *et al.* Designed Fabrication of Multifunctional Magnetic Gold Nanoshells and Their Application to Magnetic Resonance Imaging and Photothermal Therapy. Angew Chem Int Ed. 2006;45(46):7754–8.
15. Cha EJ, Jang ES, Sun IC, Lee IJ, Ko JH, Kim YI, *et al.* Development of MRI/NIRF 'activatable' Multimodal Imaging Probe Based on Iron Oxide Nanoparticles. J Control Release. 2011;155(2):152–8.
16. Josephson L, Kircher MF, Mahmood U, Tang Y, Weissleder R. Near-Infrared Fluorescent Nanoparticles as Combined MR/Optical Imaging Probes. Bioconjug Chem. 2002;13(3):554–60.
17. Dulkeith E, Morteani AC, Niedereichholz T, Klar TA, Feldmann J, Levi SA, *et al.* Fluorescence Quenching of Dye Molecules near Gold Nanoparticles: Radiative and Nonradiative Effects. Phys Rev Lett. 2002;89(20):203002.
18. Mandal SK, Lequeux N, Rotenberg B, Tramier M, Fattaccioli J, Bibette J, *et al.* Encapsulation of Magnetic and Fluorescent Nanoparticles in Emulsion Droplets. Langmuir. 2005;21(9):4175–9.
19. Sathe TR, Agrawal A, Nie S. Mesoporous Silica Beads Embedded with Semiconductor Quantum Dots and Iron Oxide Nanocrystals: Dual-Function Microcarriers for Optical Encoding and Magnetic Separation. Anal Chem. 2006;78(16):5627–32.
20. Zhang L, Liu B, Dong S. Bifunctional Nanostructure of Magnetic Core Luminescent Shell and Its Application as Solid-State Electrochemiluminescence Sensor Material. J Phys Chem B. 2007;111(35):10448–52.
21. Ma D, Guan J, Dénommée S, Enright G, Veres T, Simard B. Multifunctional Nano-Architecture for Biomedical Applications. Chem Mater. 2006;18(7):1920–7.
22. Lee S, Cha EJ, Park K, Lee SY, Hong JK, Sun IC, *et al.* A Near-Infrared-Fluorescence-Quenched Gold-Nanoparticle Imaging Probe for *In Vivo* Drug Screening and Protease Activity Determination. Angew Chem Int Ed. 2008;47(15):2804–7.
23. Cheong S, Ferguson P, Feindel KW, Hermans IF, Callaghan PT, Meyer C, *et al.* Simple Synthesis and Functionalization of Iron Nanoparticles for Magnetic Resonance Imaging. Angew Chem Int Ed. 2011;50(18):4206–9.
24. Mosmann T. Rapid Colorimetric Assay for Cellular Growth and Survival: Application to Proliferation and Cytotoxicity Assays. J Immunol Methods. 1983;65(1–2):55–63.
25. Chen F, Bu W, Chen Y, Fan Y, He Q, Zhu M, *et al.* A Sub-50 nm Monosized Superparamagnetic Fe3O4@SiO2T2-Weighted MRI Contrast Agent: Highly Reproducible Synthesis of Uniform Single-Loaded Core–Shell Nanostructures. Chemistry – An Asian. Journal. 2009;4(12):1809–16.
26. Lim CK, Kim S, Kwon IC, Ahn CH, Park SY. Dye-Condensed Biopolymeric Hybrids: Chromophoric Aggregation and Self-Assembly toward Fluorescent Bionanoparticles for Near Infrared Bioimaging. Chem Mater. 2009;21(24):5819–25.
27. Schobel U, Egelhaaf HJ, Brecht A, Oelkrug D, Gauglitz G. New Donor − Acceptor Pair for Fluorescent Immunoassays by Energy Transfer. Bioconjug Chem. 1999;10(6):1107–14.
28. LaConte LEW, Nitin N, Zurkiya O, Caruntu D, O'Connor CJ, Hu X, *et al.* Coating Thickness of Magnetic Iron Oxide Nanoparticles Affects R2 Relaxivity. J Magn Reson Imaging. 2007;26(6):1634–41.